

ANALYTICAL SOLUTION OF SEISMIC ACTIVE LATERAL FORCE IN RETAINING WALLS USING STRESS FIELDS*

A.TOTONCHI^{1**}, F. ASKARI² AND O. FARZANEH³

¹Dept. of Civil Eng., Marvdasht Branch, Islamic Azad University, Marvdasht, I. R. of Iran
Email: Arash_Totonchi@yahoo.com

²Iran International Earthquake Eng. Institute, Tehran, I. R. of Iran

³Dept. of Civil Eng., Tehran University, Tehran, I. R. of Iran

Abstract– In this paper, application of stress fields in computation of seismic active lateral forces on retaining walls is considered using the lower bound method of limit analysis. Finding the exact solution of boundary value problems in engineering fields is a complicated problem in most applied cases and from this point of view, use of the limit state methods is very beneficial for engineers. In limit analysis method, in spite of exact solution of the problem, the upper and lower bound of the limit load are determined. The lower bound of the exact solution can be obtained by use of different admissible stress fields in different regions of the media divided by stress discontinuity surfaces. Earthquakes have unfavorable effects of increasing active and decreasing passive lateral earth pressure, so to investigate how the lateral earth pressure is affected, extensive numerical results based on the limit analysis method reported by Chang and Chen. This paper is devoted to finding an Analytical solution to investigate the lateral force affection on retaining walls, using mathematical relations based on lower bound limit analysis method. This process include the calculation of direction and magnitude of active lateral earth pressure. Numerical results of the proposed algorithm are presented in some practical dimensionless graphs.

Keywords– Limit analysis, stress discontinuity surfaces, lateral pressure, retaining wall

1. INTRODUCTION

Since the earthquake motion is of an oscillatory nature, dynamic analysis of lateral earth pressure is certainly more realistic. However, dynamic analysis involves many uncertainties, e.g. the extent of soil mass effectively participating in vibrations that are not yet wholly understood.

Furthermore, providing the necessary information for a dynamic analysis and performing such an analysis are relative expensive. Quasi-Static analysis using the seismic coefficient concept is therefore of greater practical value in many cases, although the assessment of the seismic coefficient still relies highly on past experiences. The well-known Mononobe-Okabe analysis of seismic lateral earth pressure was proposed by Mononobe and Matsuo [1] and Okabe [2]. The analysis is a direct modification of the coulomb wedge analysis. In the analysis, the earthquake effects are replaced by a quasi-static inertia force whose magnitude is computed on the basis of the seismic coefficient concept. As in the coulomb analysis, the failure surface is assumed planer in the Mononobe-Okabe method, regardless of the fact that the most critical sliding surface may be curved. Similar to the coulomb's, the Mononobe – Okabe analysis may underestimate the active earth pressure and overestimate the passive earth pressure. In this paper, the lower-bound method of limit analysis is applied to include the earthquake effect which is investigated in

*Received by the editors December 30, 2010; Accepted April 15, 2012.

**Corresponding author

producing some dimensionless charts for computing the seismic active earth pressure. As stated in the lower-bound theorem, if an equilibrium state of stress below yield can be found which satisfies the stress boundary conditions, then the loads imposed can be carried without collapse by a stable body composed of elastic-perfectly plastic material [3, 4]. Any such field of stress thus gives a safe or lower bound on the collapse or limit load. The stress field satisfying all these conditions is called *statically admissible stress field*.

In this paper, the following steps are investigated: First, the lower bound of limit analysis method and the principles are defined. Second, the new formulations based on mathematical relations are introduced and a comparison between the results of this new analytical algorithm and the well-known methods such as Mononobe-Okabe is done. Finally, some practical dimensionless diagrams for calculating the active seismic coefficient of retaining walls with considerable accuracy are presented.

2. THEOREMS OF LIMIT ANALYSIS

Figure 1 shows a typical load-displacement curve as it might be measured for a surface footing test. The curve consists of an elastic portion; a region of transition from mainly elastic to mainly plastic behavior; a plastic region, in which the load increases very little while the deflection increases manifold; and finally, a work-hardening region. In a case such as this, there exists no physical collapse load. However, to know the load at which the footing will deform excessively has obvious practical importance. For this purpose, idealizing the soil as a perfectly plastic medium and neglecting the changes in geometry lead to the condition in which displacements can increase without limit while the load is held constant as shown in Fig.1. A load computed on the basis of this ideal situation is called *plastic limit load* [5, 6]. This hypothetical limit load usually gives a good approximation to the physical *plastic collapse load* or the load at which deformations become excessive. The methods of limit analysis furnish bounding estimates to this hypothetical limit load.

The theorems of limit analysis can be established directly for a general body if the body possesses the following ideal properties:

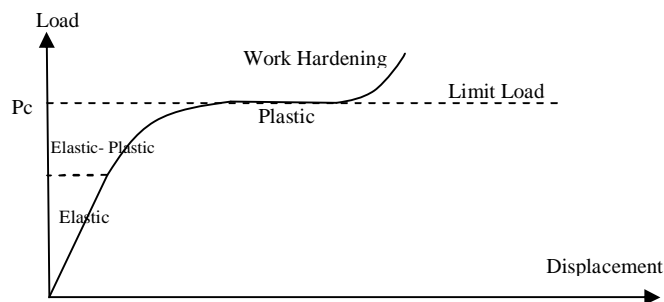


Fig. 1. Load-displacement Curve

1. The material exhibits perfect or ideal plasticity, i.e., work hardening or work softening does not occur. This implies that the stress point cannot move outside the yield surface.
2. The yield surface is convex and the plastic strain rates are derivable from the yield function through the associated flow rule.
3. Changes in the geometry of the body that occur at the limit load are insignificant; hence the equations of virtual work can be applied.

In summary, the limit load is defined as the plastic collapse load of an ideal body having the ideal properties listed above, and replacing the actual one.

3. THE LOWER BOUND METHOD

The lower-bound method of limit analysis is different from the upper-bound method in that the equilibrium equation and yield condition instead of the work equation and failure mechanism are considered [7, 8]. Moreover, whereas the development of the work equation from an assumed collapse mechanism is always clear, many engineers find the construction of a plastic equilibrium stress field to be quite unrelated to physical intuition. Without physical insight there is trouble in finding effective ways to alter the stress fields when they do not give a close bound on the collapse or limit load [9-12]. Often the user employs the existing stress fields from well-known texts or the more recent technical literature as a magic handbook and tries to fit his problem to the particular solutions he finds. Intuition and innovation seem discouraged by unfamiliarity and apparent complexity [13-14]. Although the discontinuous fields of stress which will be drawn and discussed in this Section are simpler to visualize, they too are not often employed in an original manner by the design engineer [15-16]. Yet the concepts are familiar to the civil engineer in his terms and can be utilized by the designer as a working tool.

The conditions required to establish such a lower-bound solution are essentially as follows:

- A complete stress distribution or stress field must be found, everywhere satisfying the differential equation of equilibrium.
- The stress field at the boundary and discontinuities must satisfy the stress boundary conditions.

The stress field must nowhere violate the yield condition.

4. ANALYTICAL SOLUTION

The typical 2D wall geometry for the problem of this paper is shown in Fig. 2. Assuming a discontinuity surface, Fig. 2 shows the variation of stresses in the vicinity of the wall (zone A) and beyond the discontinuity surface (zone B). The final target of the calculations is leads to the evaluation of P_{ah} and P_{av} which are the stresses subjected to the earthquake affected on the wall. In this solution the following relation is assumed.

$$\frac{C_w}{C} = \frac{\tan(f_w)}{\tan(f)}$$

In which, c and ϕ are known as the strength parameters of the material; c represents the *cohesion* and ϕ represents the *angle of internal friction*. c_w is the cohesion and ϕ_w is the internal friction angle between the wall and soil. Knowing the stresses quantities in element B, Fig. 3 is drawn.

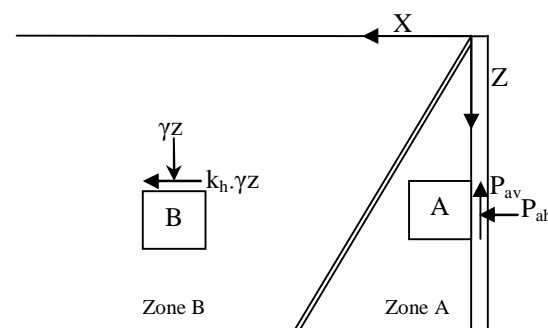


Fig. 2. Stress discontinuity surface, zones A and B

The Mohr circle center and radius are considered as S_a, S_b and r_a, r_b respectively for zones A and B.

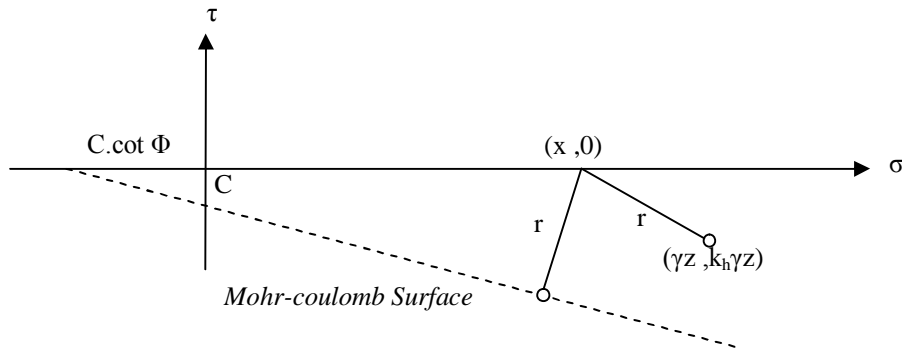


Fig. 3. Assuming S_b as $(x, 0)$

$$r = (x + C \cdot \cot(f)) \cdot \sin(f) \tag{1}$$

$$r = \sqrt{(g \cdot z - x)^2 + (K_h \cdot g \cdot z)^2} \tag{2}$$

Combining (1) & (2) results in:

$$(x + c \cdot \cot(f))^2 \cdot \sin^2(f) = (g \cdot z)^2 + (x)^2 - (2gz) \cdot (x) + (k_h \cdot gz)^2 \tag{3}$$

Expanding Eq. (3) leads to:

$$(x)^2(\sin^2 f - 1) + x(2c \cdot \cos f \cdot \sin f + 2gz) + (c^2 \cos^2 f - (k_h \cdot gz)^2) = 0 \tag{4}$$

Where $x = S_b$. As S_b and r_b are calculated, the Mohr circle of zone-B is drawn (Fig. 4).

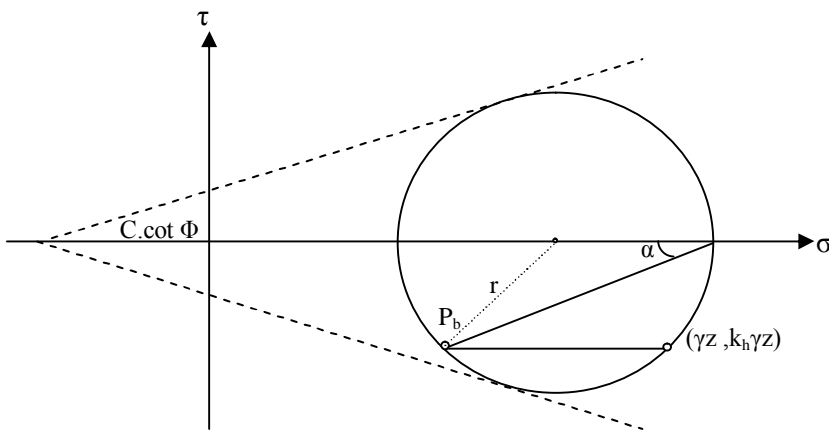


Fig. 4. Mohr circle in zone part B

The soil is modeled by Mohr-Coulomb yield criterion with various quantities of friction angle and soil cohesion. In a direct application of the Mohr-Coulomb criterion for plane strain stability problems, it is implicitly assumed that the strength of the soil along the failure surface is fully mobilized everywhere along the surface. This is probably the case in most laboratory tests in which the tested specimen is assumed representative of a soil element in the soil mass. This is because the specimen is generally so small that the strain is practically considered uniform along the failure surface, although boundary restrains do exist in almost all tests. For simplicity, the effect of seepage (or pore pressures) on the stability of cohesive-frictional soils has not been included in this study. It is also possible to incorporate the effect of pore pressures in limit analysis [17, 18], but this extension is not being covered here. The

position of stresses of zone B is shown in Fig. 3. The relation of Mohr circle center and radius of zone-B can be expressed by:

In Fig. 4 P_b is the pole of Mohr circle of zone-B. For computation of the angle between P_b and the principle surface (α) in the Mohr-circle of zone B, using geometrical relations leads to the following equations:

$$\tan(\alpha) = \frac{k_h \cdot g \cdot z}{|g \cdot z - s_b| + r} \tag{5}$$

Substituting r_b in the above equation leads to:

$$\alpha = \tan^{-1} \left(\frac{K_h \cdot \gamma z}{|\gamma z - s_b| + \sqrt{(\gamma z - s_b)^2 + (K_h \cdot \gamma z)^2}} \right) \tag{6}$$

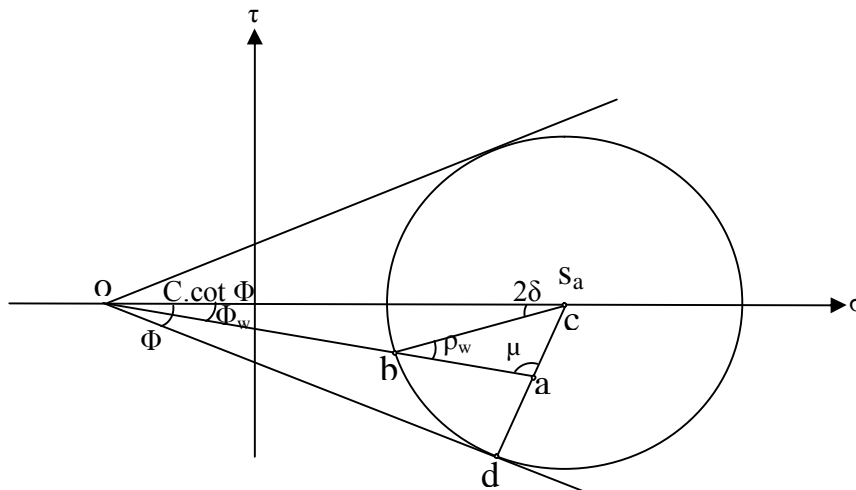


Fig. 5. Assumed Mohr circle in zone part A

Dismounting the wall specifications, the Mohr-circle of zone-A is drawn (Fig (5)). Using Fig (5) results in the following equations:

$$\frac{ac}{\sin(r_w)} = \frac{bc}{\sin(m)} \tag{7}$$

$$\frac{ac}{\sin(f_w)} = \frac{oc}{\sin(m)} \Rightarrow \sin(m) = \frac{oc \cdot \sin(f_w)}{ac} \tag{8}$$

$$\frac{dc}{\sin(f)} = \frac{oc}{\sin(90)}$$

$$dc = bc$$

$$\Rightarrow \frac{bc}{\sin(f)} = \frac{oc}{1}$$

$$\sin(f) = \frac{bc}{oc} \tag{9}$$

Combining (4) & (6) results in:

$$\sin(r_w) = \frac{ac}{bc} \cdot \sin(m) \text{ \& } \sin(r_w) = \frac{ac}{bc} \cdot \frac{oc}{ac} \cdot \sin(f_w)$$

$$\sin(r_w) = \frac{oc}{bc} \cdot \sin(f_w)$$

$$\sin(r_w) = \frac{\sin(f_w)}{\sin(f)} \tag{10}$$

$$r_w = 2d + f_w$$

$$d = \frac{r_w - f_w}{2} \tag{11}$$

Considering β as an angle through zone-A stresses surface and principle surface, the rotation angle of stresses from zone A to B will become:

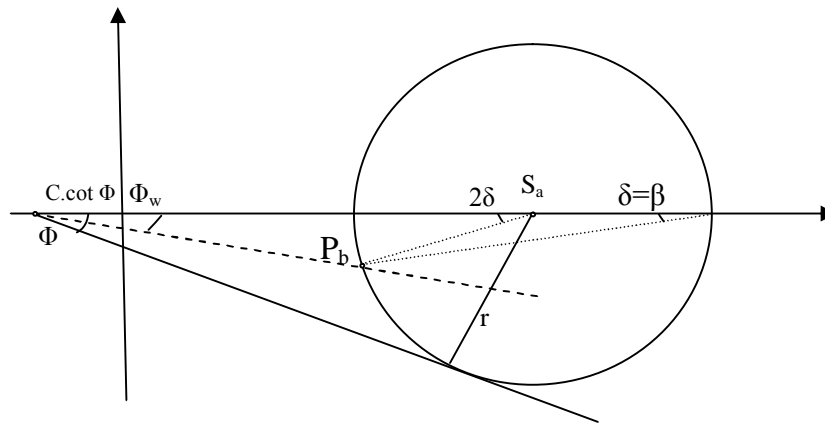


Fig. 6. β recognition for calculating the rotation angle of stresses from zone B to A

$$b = d = \frac{r_w - f_w}{2} \tag{12}$$

From Figs. 5 and 6, $\delta\theta$ is defined as the following equation (Fig (7)):

$$dq = b - a$$

Substituting α and β in the above equation leads to:

$$dq = \frac{r_w - f_w}{2} - \tan^{-1}\left(\frac{k_h \cdot g \cdot z}{|g \cdot z - s_b| + r}\right) \tag{13}$$

In which $\delta\theta$ is rotation angle of stresses from zone B to A. Using the relation between the two center points of the Mohr-circles of zones A and B, reported by Chen and Chung [19], following equations are derived.

$$\frac{s_b + c \cdot \cot(f)}{s_a + c \cdot \cot(f)} = \frac{\cos(dq - r)}{\cos(dq + r)} \tag{14}$$

$$\sin(r) = \cos(dq) \cdot \sin(f) \tag{15}$$

$$r_a = (s_a + c \cdot \cot(f)) \cdot \sin(f) \tag{16}$$

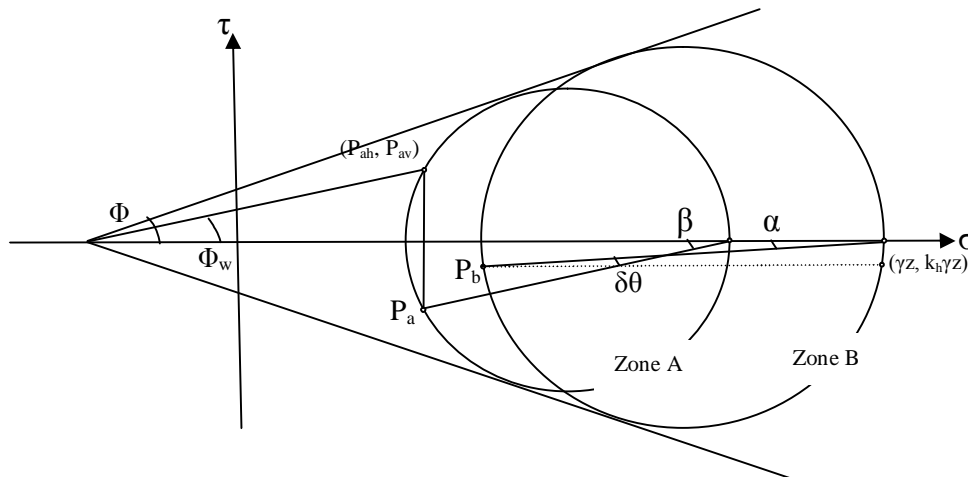


Fig. 7. $\delta\theta$ recognition (rotation angle of stresses from zone B to A)

Knowing the quantities of the r_a and S_a , Mohr-circle of element A is drawn. According to Fig.8, depicted by a line through the intersection point of circles (M) and pole B (P_b) and extending it, the pole of the Mohr-circle in zone A appears, which leads to attaining the target.

In summary, the calculation algorithm of p_{ah} is defined as follows:

- 1- Calculation of S_b , r_b and α using Eqs. (2), (4) and (6).
- 2- Calculation of β using Eq. (12).
- 3- Determining the rotation angle between the Mohr-circles ($\delta\theta = \beta - \alpha$) then use of Eqs. (14) and (16) for calculation of S_a and r_a , respectively.
- 4- Drawing the Mohr-circles, finding the pole of the element in zone A which leads to the calculation of p_{ah} .

The next section discusses the comparison of this mathematical solution and Mononobe-Okabe Method which results in some tables and graphs.

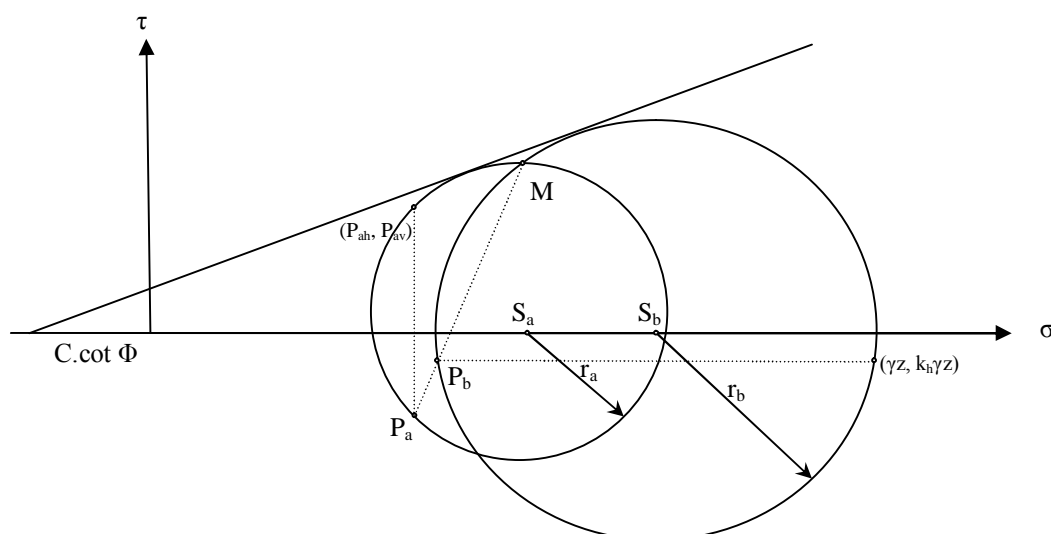


Fig. 8. Computation of active seismic stresses on retaining wall

5. COMPARISON BETWEEN RESULTS

The Mononobe-Okabe analysis [20, 21], which is an extension of the coulombs analysis, has been experimentally proved by Mononobe-Matsuo [4, 6] to be effective in assessing the seismic active earth pressure. It is generally adopted in the current a seismic design of rigid retaining walls. The Mononobe-Okabe solution is therefore practically acceptable, at least for the active pressure case, although its applicability to the passive pressure is somewhat in doubt.

In this section, some results on seismic active pressures as obtained by the present *Analytical method* are compared with the method of Mononobe-Okabe (M-O), which leads to tables 1 to 4. Comparing the current results with these methods, good agreement is found among them.

In the following tables, k_h is horizontal seismic coefficient, δ is friction angle between the wall and soil in the Mononobe-Okabe method and K_{AE} is active seismic lateral pressure coefficient.

Table 1. Comparison of K_{AE} for $C=0$, $\Phi_w=\Phi/2$, $K_h=0.15$, $K_v=.075$, $H=5$ m, $\gamma=17.6$ kN/m³

Φ	δ	K_{AE}	K_{AE}
	Φ_w	M-O	Analytical Solution
10	5	0.928	0.926
16	8	0.697	0.693
20	10	0.598	0.598
26	13	0.481	0.481
28	14	0.448	0.446
30	15	0.417	0.416
32	16	0.389	0.386
36	18	0.337	0.337
38	19	0.313	0.311
40	20	0.292	0.292

Table 2. Comparison of K_{AE} for $C=0$, $\Phi_w=\Phi/2$, $H=5$ m, $\gamma=17.6$ kN/m³

K_h	Φ	Φ_w	K_{AE}	
			M-O	Analytical solution
0.1	30	15	0.373	0.373
0.2	30	15	0.467	0.466
0.3	30	15	0.595	0.595
0.1	10	5	0.795	0.795
0.2	10	5	1.036	1.036
0.3	10	5	0.996	0.996
0.1	40	20	0.257	0.257
0.2	40	20	0.33	0.33
0.3	40	20	0.425	0.425

So it has been found that the application of limit analysis for cohesionless soil stability problems is practically acceptable. The determination of the seismic lateral earth pressure of a fill on a retaining wall, when frictional forces act on the back of the wall, is solved conveniently by this analytical method.

As seen, the results of Analytical solution and Mononobe-Okabe are practically identical for most cases. By checking the results of Chung & Chen, which are based on upper bound method of limit analysis, it seems that the exact result has a negligible difference with the results of this method.

Table 3. Comparison of K_{AE} for $C=0$, $\Phi_w=\Phi/2=15^\circ$, $H=5$ m, $\gamma=17.6$ kN/m³

K_h	Analytical Solution	M-O	Chen and Chung
0.1	0.373	0.373	0.4
0.2	0.466	0.467	0.49
0.3	0.595	0.595	0.62

Table 4. Comparison of active lateral pressure for $\Phi=30^\circ$, $\gamma=18$ kN/m³

C(kPa)	Z(Meter)	Rankin	Analytical
10	0	-11.489	-11.455
	10	47.91	47.788
20	0	-22.978	-22.97
	10	36.421	36.419
30	0	-34.467	-34.454
	10	24.932	24.912

6. NUMERICAL RESULTS

The lower bound solutions obtained can be applied directly in practice and one of the most usable applications of this study is the possibility of introducing some practical dimensionless diagrams for calculating the active seismic lateral pressure coefficient of retaining walls with considerable accuracy. Figures 9 to 11 illustrate the active seismic lateral force in various quantities of friction angle and cohesion of the soil and soil-wall. The dimensionless parameters presented are defined as:

$$l = gH / c$$

$$P' = P / Hc$$

Where γ is soil unit weight, H is the wall height, c is the cohesion of the soil fill at the back of the wall and P is the seismic lateral force which affects the wall. For each seismic coefficient, the results for three different λ of 3, 5 and 10 are given. To account for the effect of c_w and Φ_w , the results are presented in terms of c_w of 0.2, 0.3 and 0.8. As Figs. 9 to 11 show, by increasing the soil friction angle, the seismic active force is decreased, as expected. Comparing Figures, it seems that for a given λ the active seismic force will increase with increasing c_w/c . Also, it seems that increasing in λ and k_h , leads to increase the seismic lateral force (P).

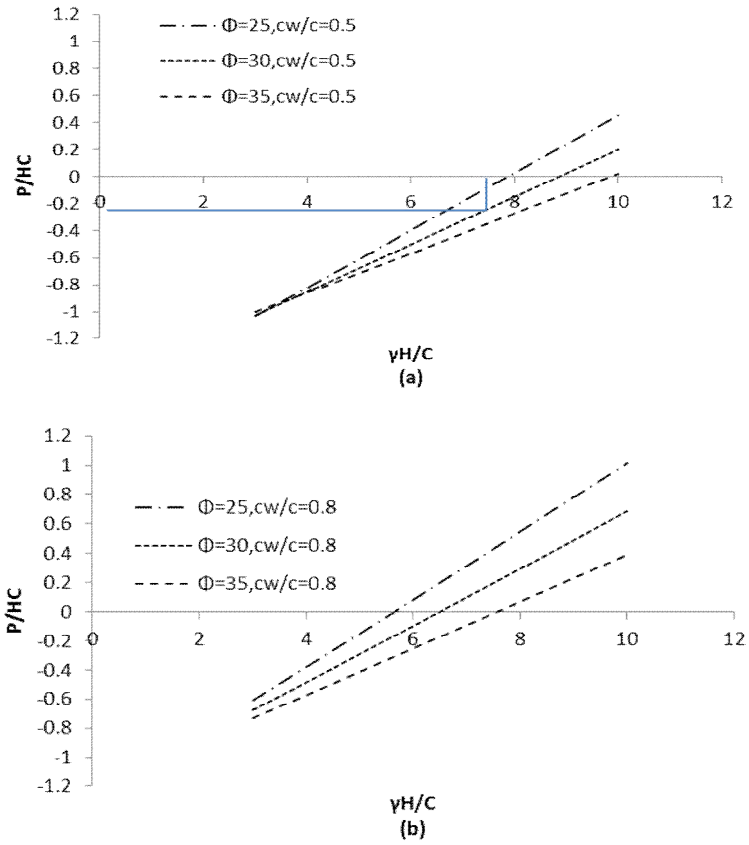


Fig. 9. Dimensionless diagram for calculating the active seismic lateral force, $K_h=0.1$

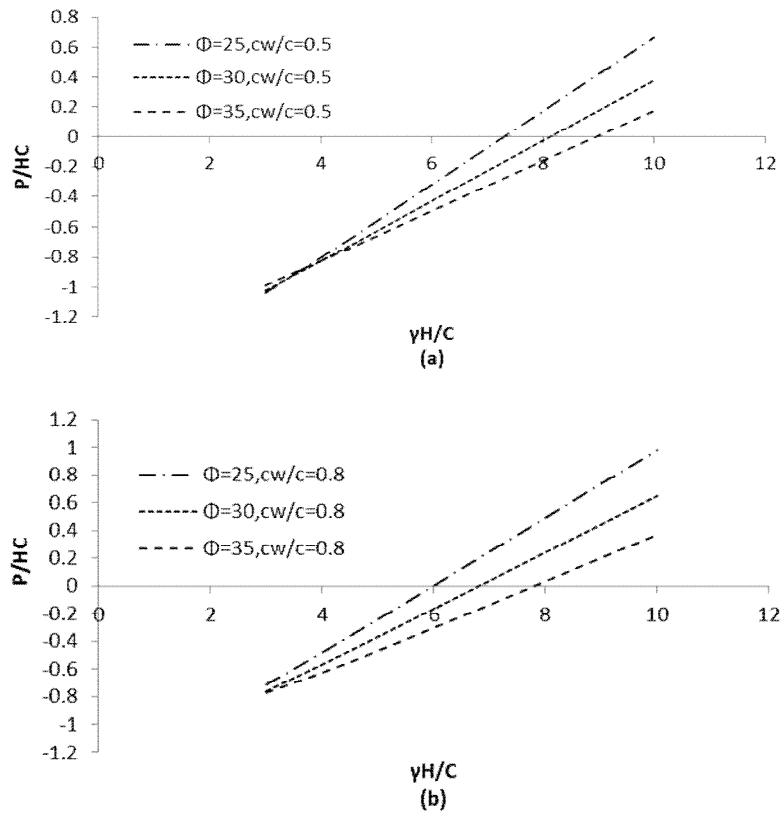


Fig. 10. Dimensionless diagram for calculating the active seismic lateral force, $K_h=0.2$

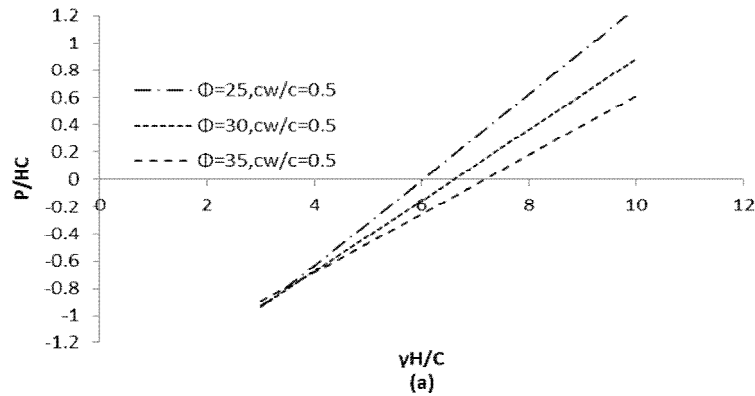


Fig. 11. Dimensionless diagram for calculating the active seismic lateral force, $K_h=0.3$

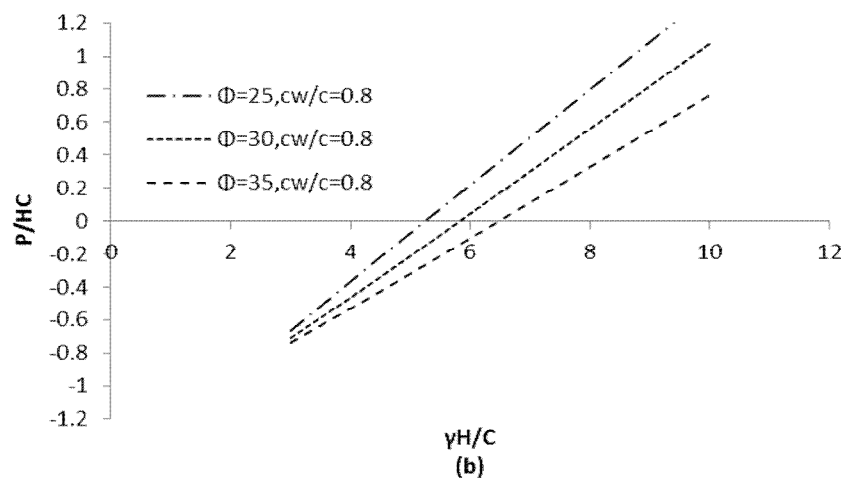


Fig. 11. Dimensionless diagram for calculating the active seismic lateral force, $K_h=0.3$, (Continue)

7. EXAMPLE OF APPLICATION

Now, how the results in Figs. 9 to 11 can be used to determine the seismic active lateral force is illustrated.

Problem. A wall is built back of a soil which has the following parameters, the height of the wall $H=5$ m, the soil unit weight is $\gamma=15$ kN/m³, the soil's strength parameters $c=10$ kN/m², $\Phi=30$ and the soil-wall cohesion $c_w=5$ kN/m². For a seismic coefficient of $k_h=0.1$, what is the amount of *seismic active lateral force*?

A procedure for using the results of the presented study to solve the forgoing problem can be summarized as follows:

- 1- From the value of γ , H and c , the dimensionless parameter $\lambda=\gamma H/c=7.5$ is calculated.
- 2- With $k_h=0.1$ and $c_w/c=0.5$, it follows that the results presented in Fig. 9a should be used to determine the force.
- 3- In Fig. 9a, a straight-vertical line passing through $\lambda=7.5$ is drawn. This straight line will intersect with three curves from which the intersection point of curve with $\Phi=30$ and $c_w/c=0.5$ is selected.
- 4- From this intersection point, it can back-figure the following dimensionless parameter P' from which the lower bound solution of the seismic active force can be calculated as $P=-11.23$ kN/m.

8. CONCLUSION

The active seismic lateral pressure on the retaining wall is investigated in this paper. An *Analytical* solution is introduced based on lower bound limit analysis method and the solution is compared to the well-known methods such as Mononobe- Okabe and Chung and Chen, whose results are close to each other. Some practical dimensionless diagrams for calculating the active seismic coefficient of retaining walls with considerable accuracy are presented. The results show that by increasing the soil friction angle, the seismic active force is decreased, as expected. Comparing diagrams, it seems that for a given $\lambda = \gamma H/c$ the active seismic force will increase with increasing c_w/c . Also, it is found that an increase in λ and k_h , leads to an increase in the seismic lateral force.

NOMENCLATURES

c	cohesion
c_w	cohesion between soil and wall
Φ	internal friction angle
Φ_w	internal friction angle between soil and wall
γ	soil unit weight
z	height
P_{av}	vertical active seismic lateral pressure
P_{ah}	horizontal active seismic lateral pressure
S_a	center point of Mohr-circle in zone A
S_b	center point of Mohr-circle in zone B
r_a	radius of Mohr-circle in zone A
r_b	radius of Mohr-circle in zone B
P_a	pole of zone-A
P_b	pole of zone-B
α	angle between P_b and the principle surface
β	angle between P_a and the principle surface
$\delta\theta$	rotation angle of stresses from zone B to A
M	Intersection of Mohr-circles
K_h	Seismic coefficient
λ	dimensionless parameter $=\gamma H/c$
P	seismic lateral force
p	dimensionless parameter $=p/Hc$

REFERENCES

1. Mononobe, N. & Matsou, H. (1929). *On the determination of earth pressure during earthquake. Proceedings, World Engineering Congress*, p. 9.
2. Okabe, S. (1926). *General theory of earth pressure. Journal of the Japan Society of Civil Engineering*, Vol. 12, No. 1.
3. Collins, I. F. (2005). Elastic/plastic models for soils and sands. *Int. J. Mech. Sci.* Vol. 47, pp. 493–508.
4. Drucker, D. C. & Prager, W. (1952). Soil mechanics and plastic analysis for limit design. *Quart. Appl. Math.*, Vol. 10, pp. 157–165.
5. Burland, J. B., Rampello, S., Georgiannou, V. N. & Calabresi, G. (1996). *A laboratory study of the strength of four stiff clays. Geotechnique*, Vol. 46, No. 3, pp. 491–514.
6. Chen, W. F. & Han, D. J. (1988). *Plasticity for structural engineering*. Springer, New York.
7. Atkinson, J. H. (1981). *Foundation and slopes, an introduction to applications of critical state soil mechanics*. McGraw-Hill Company.
8. Kramer, S. L. (1996). *Geotechnical earthquake engineering*. Uni. of Washington, Prentice Hall

9. Drucker, D. C., Prager, W. & Greenberg, H. J. (1952). Extended limit design theorems for continuous media. *Quart. Appl. Math.*, Vol. 9, pp. 381–389.
10. Fleck, N. A. & Hutchinson, J. W. (1993). A phenomenological theory for strain gradient effects in plasticity. *J. Mech. Phys. Solids*, Vol. 41, No. 12, pp. 1825–1857.
11. Toupin, R. A. (1962). Elastic materials with couple stresses. *Arch. Ration. Mech.*, Vol. 11, pp. 385–414.
12. Vardoulakis, I. & Graf, B. (1985). Calibration of constitutive models for granular materials using data from biaxial experiments. *Geotechnique*, Vol. 35, pp. 299–317.
13. Vardoulakis, J., Labuz, J. F., Papamichos, E. & Tronvoll, J. (1998). Continuum fracture mechanics of uniaxial compression on brittle materials. *Int. J. Solids Struct.*, Vol. 35, Nos. 31–32, pp. 4313–4335.
14. Zhao, J. D., Sheng, D. C. & Zhou, W. Y. (2005). Shear banding analysis of geomaterials by strain gradient enhanced damage model. *Int. J. Solids Struct.* Vol. 42, No. 20, pp. 5335–5355.
15. Li, A.J. & Lyamin, A. V. (2009). Seismic rock slope stability charts based on limit analysis methods. *Computers and Geotechnics*, Vol. 36, pp. 135-148
16. Merifield, R. S. & Lyamin, A. V. (2006). Limit analysis solutions for the bearing capacity of rock masses using the generalized Hoek–Brown criterion. *International Journal of Rock Mechanic Mining Science*, Vol. 43, pp. 920–37.
17. Anvar, S. A. & Gharamani, A. (1997). Equilibrium equations on zero extension lines and its application to soil engineering. *Iranian Journal of Science & Technology, Transaction B*, Vol. 21, No. 1, pp. 11-34
18. Jahanandish, M. & Eslami haghightat, A. (2004). Analysis of Boundary value problems in soil Plasticity Assuming Non-Coaxiality. *Iranian Journal of Science & Technology, Transaction B*, Iranian Journal of Science & Technology, Transaction B, Vol. 28, No. B5.
19. Chen, W. F. & Liu, X. L. (1990). *Limit analysis in soil mechanics*. West Lafayette.
20. Hack, R. Alkema, N. & Luzi, L. (2007). Influence of earthquakes on the stability of slopes. *Eng. Geol.*, Vol. 91, pp. 4–15.
21. Shou, K. J. & Wang, C. F. (2003). Analysis of the Chiufengershan landslide triggered by the 1999 Chi-Chi earthquake in Taiwan. *Eng. Geol.*, Vol. 68, pp. 237–50.